VYSOKÉ UČENÍ TECHNICKÉ V BRNĚ
Fakulta strojního inženýrství
Ústav fyzikálního inženýrství

Mgr. Alexandr Jonáš

USE OF STANDING ELECTROMAGNETIC WAVE FOR MANIPULATION OF MICRON AND SUBMICRON-SIZED OBJECTS

VYUŽITÍ STOJATÉ ELEKTROMAGNETICKÉ VLNY PRO MANIPULACI S OBJEKTY MIKROMETROVÝCH A SUBMIKROMETROVÝCH ROZMĚRŮ

SHORT VERSION OF PHD THESIS

Obor: Fyzikální a materiálové inženýrství

Školitelé: RNDr. Pavel Zemánek, Ph.D.
prof. RNDr. Miroslav Liška, DrSc.

Oponenti: doc. RNDr. Zdeněk Bouchal, Dr.
RNDr. Radim Chmelík, Ph.D.
RNDr. Stanislav Kozubek, DrSc.

Datum obhajoby: 13. listopadu 2001

KEY WORDS

optical trapping, light scattering, optical forces, light microscopy, noise analysis

KLÍČOVÁ SLOVA

optické zachytávání, rozptyl světla, optické síly, světelná mikroskopie, šumová analýza

MÍSTO ULOŽENÍ PRÁCE

Knihovna FSI VUT v Brně

© 2001 Alexandr Jonáš
ISBN 80-214-2021-9
ISSN 1213-4198

CONTENTS

1 PRESENT STATE 5

2 AIMS OF THE Ph.D. THESIS 6

3 MAIN METHODS AND RESULTS 6

3.1 Theoretical determination of radiation forces 6

3.1.1 Forces on an irradiated spherical particle of general size and refractive index 6

3.1.2 Radiation forces in limiting cases 7

3.2 Optical trapping in Gaussian standing wave 8

3.2.1 Generation and features of Gaussian standing wave 8

3.2.2 Characterisation of the Gaussian standing wave optical trap 9

3.3 Practical realisation of the standing wave trap 16

3.3.1 Experimental set-up for the optical confinement and micromanipulation 16

3.3.2 Measurement of the optical trap stiffness 18

3.3.3 Coexistence of the single beam and standing wave trapping 23

4 CONCLUSION 25

5 ZÁVĚR 26

6 REFERENCES 28

7 CURRICULUM VITAE 30

1 PRESENT STATE

Since the first experiments of Arthur Ashkin in early 1970's, which demonstrated the possibility of moving and even stable spatial fixation of an immersed dielectric particle with the use of two counter-propagating continuous laser beams [1], the manipulation of micron and submicron-sized objects by light (*optical trapping*) has found its way to various branches of research. The present applications of optical forces range from the study of the mechanical properties of single cells [2], single molecules [3, 4], measurement of the interaction forces between particles and various surfaces [5] to the construction of novel types of the local probe microscopes [6, 7] and study of chemical reactions and spectroscopy in micron-sized domains [8]. Such a broad application spectrum follows from the fact that an optical trap is not only a means for shifting of trapped dielectric objects but it can also serve to quantify external forces acting on these objects [9].

In general, presently used optical traps are almost exclusively based on the exploitation of the strong optical intensity gradients in the inhomogeneous light wave incident upon a target object. In such a field, an object surrounded by an optically less-dense medium is attracted towards the point of the highest optical intensity due to the effect of the dielectric polarisation [10]. First full-optical gradient trap for macroscopic particles (so-called *optical tweezers*) was presented by A. Ashkin *et al.*, who used a single TEM_{00} laser beam tightly focused by a high numerical aperture microscope objective to trap submicron colloidal silica particles [11]. With several modifications of Ashkin's original set-up involving e.g. higher-order mode (TEM_{01}^{*}, TEM_{01}) beams [12], optical fibres [13] and multi-beam trap systems [14], optical tweezers has nowadays become the most widely spread trapping scheme. Such a trap, however, suffers from a notable asymmetry in the axial and transversal directions with the axial forces being several times smaller [15]. This is an inherent feature given by physical restrictions, which are imposed upon the spatial light intensity distribution created by focusing system with limited numerical aperture. To overcome this disadvantage, a method was suggested in the author's home laboratory at the Institute of Scientific Instruments, which is based on the use of the *Gaussian standing wave* (GSW) created by superposition of two counter-propagating coherent beams [16,17]. One of these beams is generated by retro-reflection from a planar surface, which is perpendicular to the propagation direction of the incident beam. In the standing wave, the neighbouring intensity maxima (antinodes) or minima (nodes) are separated by half the wavelength. During the shift from the GSW node to antinode, the intensity changes from the minimal to the maximal value on the distance of a quarter of wavelength. Such a steep intensity change is then accompanied by axial intensity gradients and associated forces, which can be by several orders of magnitude higher than those achieved with a single focused beam [16]. Moreover, periodic nature of the standing wave enables in principle to confine several objects simultaneously [17].

2 AIMS OF THE Ph.D. THESIS

The aim of the presented Ph.D. thesis is the theoretical and experimental study of the optical trapping in the reflection-generated GSW for various parameters of the trapping system. The standing wave trap optical forces and other characteristics (trap stiffness, trap depth) are calculated for various parameters of the trapped object (size, refractive index), trapping laser beam (focal spot size, distance of the focal spot from the reflective surface), and reflective surface (reflectivity). Comparison with the corresponding features of the single beam trap is done that demonstrates the standing wave trap superiority. An experimental system for the practical realisation of the standing wave trap is introduced and a comparative measurement of the standing wave and single beam trap stiffness is presented. The coexistence of the two trapping mechanisms for certain configurations of the experimental system is studied and the presence of a weakly modulated standing wave component of the total field in the vicinity of an ordinary glass-water interface is proved.

3 MAIN METHODS AND RESULTS

3.1 Theoretical determination of radiation forces

Our goal is the calculation of the forces acting on a spherical dielectric object immersed in a dielectric fluid and irradiated by a time-varying electromagnetic field. This can be done by introducing the concept of the stress tensor of electromagnetic field in a dielectric medium [10]. The resulting forces acting on the immersed sphere are then given by the integral of the stress tensor over a closed surface surrounding the sphere [10]. Alternatively, analytical formulas for the optical forces can be derived when the parameters of the dielectric sphere (size, relative refractive index) are restricted [15,18,19].

3.1.1 Forces on an irradiated spherical particle of general size and refractive index

The stress tensor can be constructed if the field vectors **E**, **D** (electric intensity and displacement) and **B, H** (magnetic induction and intensity) are known on the integration surface (see above). This requires solving the problem of the *scattering* of the incident wave by the irradiated object [20]. For a sphere of arbitrary size irradiated by a plane monochromatic wave, this was already achieved in the beginning of the twentieth century by G. Mie, P. Debye and L. Lorenz, who expressed the desired solution in the form of infinite series with appropriate expansion coefficients [21]. Extension of their approach within the framework of so-called *generalised Lorenz-Mie theory (GLMT)* enables to treat the case of a laser beam of an arbitrary shape. The only difference is in the complexity of the infinite series and the number of expansion coefficients, which have to be evaluated [22]. The net radiation force can be then expressed in the form of infinite series constituted by the field expansion coefficients [23].

3.1.2 Radiation forces in limiting cases

If the range of the trapped particle size or refractive index is restricted, approximate procedures leading to closed analytical formulas for trapping forces can be used. These analytical expressions can considerably shorten the necessary computation time and even if they are stretched beyond their validity limits, they can still provide at least qualitative information on general trends.

If the radius *a* of the trapped dielectric sphere is much smaller than the radiation wavelength λ in the immersion medium (practical limit is $a < \lambda /20$ [20]), it can be treated as an elementary induced dipole, which scatters isotropically the incident field (Rayleigh scattering). The interaction of such a Rayleigh scatterer with the field then manifests itself through two types of forces: the gradient force coming from electrostatic interaction with inhomogeneous incident field and the scattering force, which is due to the redistribution of the net electromagnetic momentum [18]. The gradient force points, for particles surrounded by an optically less dense medium (particle refractive index n_{int} is greater than the refractive index of immersion n_{ext}), in the direction of the intensity gradient i.e. it attracts the particle to the intensity maximum. Purely axial scattering force pushes the particle in the incident wave propagation direction. The possibility of the stable confinement in the axial direction is then given by the balance of the two force components and it requires strong axial intensity gradients.

On the other hand, if the particle radius *a* is so big that the actual wavelength of trapping radiation becomes irrelevant, the description of the particle-wave interaction can be done within the framework of geometrical (ray) optics [15]. In the ray optics domain, the incident wave is formally represented by a bundle of rays carrying specific momentum, which impinge upon the particle, reflect from it and refract into its interior. This process leads to the change of momentum of the ray bundle and, consequently, change of the particle momentum due to the radiation force.

Finally, let us consider a particle, whose refractive index is close to the one of the immersion medium. Generally, when a dielectric particle is placed into an inhomogeneous electromagnetic field, which exists in a dielectric immersion liquid, the field distribution and consequently the total energy of the field inside the liquid changes. In case that both the particle and immersion liquid are nonmagnetic and the particle is only weakly polarised, i.e. $m = n_{int} / n_{ext} \rightarrow 1$, the interaction energy change can be expressed using solely the original (unperturbed) field [19]. Time-averaged force acting on the particle is then done by the gradient of interaction energy.

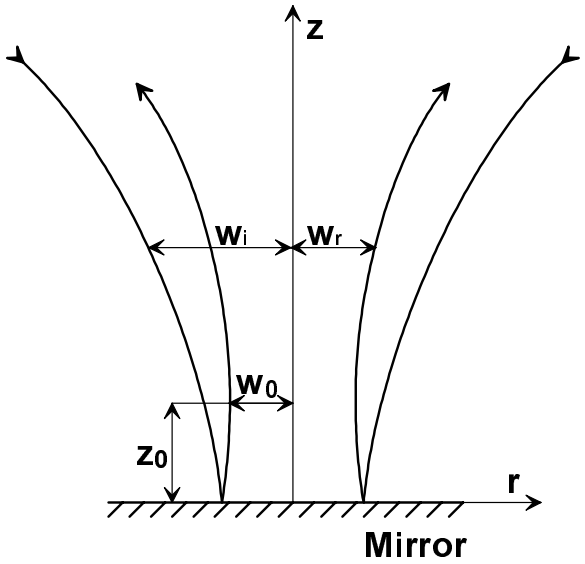

Figure 1. Generation of Gaussian standing wave by reflection of the incident laser beam from the mirror. z axis follows the direction of the reflected wave and z_0 is the position of the beam waist (positive for the beam waist created in the reflected wave).

3.2 Optical trapping in Gaussian standing wave

3.2.1 Generation and features of Gaussian standing wave

A standing wave is generally created by interference of two counter-propagating coherent waves. In the method, which was suggested and experimentally realised by our group [16,17], these two coherent waves are obtained as the result of retroreflection of the incident laser beam from a highly reflective coated slide (mirror). Schematically, this is illustrated in Fig. 1. For the calculations, both beams are described using the fifth-order corrected Gaussian beam model [24]. The beam radius at the focal plane (the beam waist) is w_0 and the focal plane is located at distance z_0 from the mirror, which is positive for the beam focus in the reflected wave and negative for the focus in the incident wave. The effect of reflection is described by a single complex-valued Fresnel reflection coefficient $r_m = \rho\, exp(-i\psi)$, where ρ determines the amplitude attenuation of the reflected wave and ψ is the phase shift of the reflected wave.

An example of the GSW intensity distribution is given in Fig. 2a. Because the intensity in the standing wave changes in axial direction from minimal value (zero in an ideal case) to maximal value on the distance of a quarter of wavelength, strong axial intensity gradients are generated. As already mentioned, these gradients are the origin of stabilising gradient forces, which facilitate spatial confinement of a dielectric object in an optically less-dense medium. The magnitude of these gradients then depends on the standing wave modulation depth, which in turn is given by the ratio of amplitudes of both interfering beams. For comparison, intensity profile of a single focused beam with the same parameters (i.e. beam waist size w_0 and total power P) is shown in Fig. 2b. As can be seen, there is only a minor

difference in the transversal gradients (they differ maximally by a factor of 4, which - for equal width of intensity distributions - stems from the amplification of the on-axis intensity by interference in the GSW [16]). In the axial direction, however, the GSW gradients dominate over the single beam ones by several orders of magnitude, as the slow fall of the single focused beam intensity cannot compete with rapid oscillations of the interference structure. This qualitative prediction implies much better axial stability of the optical trapping in the standing wave in comparison with single beam trapping.

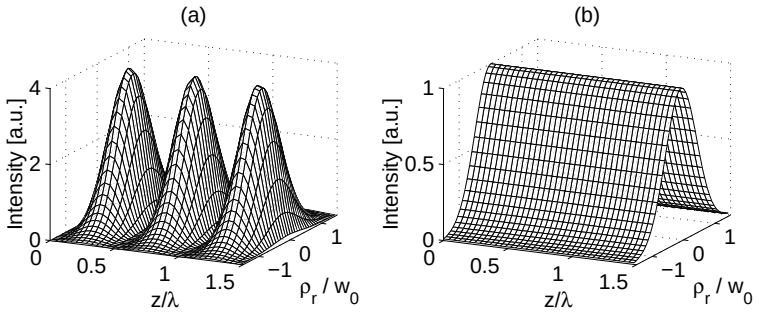

Figure 2. An example of intensity distribution in the standing wave (a) and single focused beam (b) for the same beam waist size and total power in the incident laser beam. Fixed parameters: $w_0 = 3\lambda$, $z_0 = 0\ \mu m$, $\lambda_{vac} = 1064\ nm$, $\rho = 1$, $\psi = \pi$.

3.2.2 Characterisation of the Gaussian standing wave optical trap

An optical trap containing a confined dielectric object can be characterised by the magnitude of the optical forces exerted upon the object and other parameters, such as the minimal power required to obtain stable trapping and the trap stiffness. With the use of the previously presented procedure, all these characteristics for the standing wave trapping can be calculated and compared with the corresponding features of the classical single beam trap for various particle and incident beam parameters. Because the optical intensity distributions in the single beam and standing wave differ substantially only in the axial direction (see Fig. 2), it is sufficient to concentrate merely on the study of the axial features of both types of optical traps.

Standing wave trapping forces

The magnitude of optical forces and their distribution in the electromagnetic field are the basic parameters of an optical trap. A qualitative picture of the trapped particle behaviour can already be obtained from the concept of gradient and scattering forces and the knowledge of the optical intensity distribution. The only transversal force component is the gradient force, which - for particles with relative refractive index $m>1$ - points towards the highest intensity region [18]. Consequently, in the considered case of Gaussian standing wave (or single focused Gaussian beam), such particle is always pulled towards the optical axis of the incident beam. In the axial direction, the existence of equilibrium is conditioned by achievement of balance of the gradient and scattering forces. If the optical intensity

gradient is insufficient, the particle is accelerated in the incident beam direction by the scattering force and stable trapping cannot be achieved.

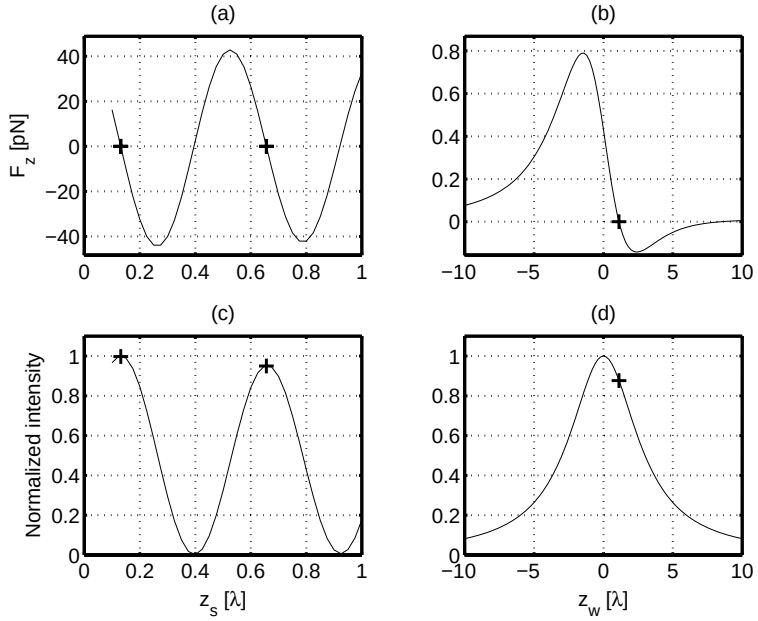

Figure 3. Comparison of the axial trapping forces in the standing wave trap and single beam trap. In the top row, standing wave force plotted against the distance z_s of the particle from the reflective surface (a) and single beam force plotted against the distance z_w of the particle from the beam waist (b) are shown. In the bottom row, corresponding profiles of optical intensity (c), (d), respectively, are presented. Crosses denote stable equilibrium positions of the particle. Fixed parameters: $a = 0.1\lambda = 80$ nm, $m = 1.19$, $w_0 = 1\ \lambda$, $z_0 = 0\ \mu m$, $P = 1W$, $\lambda_{vac} = 1064$ nm, $n_{ext} = 1.33$, $\rho = 1$, $\psi = 3\pi/2$.

An example of the standing wave axial force profile calculated with the use of the GLMT is shown in Fig. 3a. The chosen relative refractive index of the particle *m* corresponds to polystyrene immersed in water, which is frequently used in experiments. Oscillations, which can be observed in the force pattern, are associated with the periodical interference structure of the standing wave. For comparison, the single beam force profile for the same parameters of the trapping system (particle size and refractive index, beam waist size and total beam power) is shown in Fig. 3b. We can see immediately that, in the latter case, the optical force is by two orders of magnitude smaller. This can be readily explained by comparison of the standing wave and single beam intensity profiles (see Fig. 3c,d), which reveals approximately two-order difference between the steepness of the single beam and the standing wave intensity gradients (note different scale of *z* co-ordinate of both plots). The stable equilibrium position of the particle in the optical field is located at the place, where the force is zero and the slope of the force with respect to the axial co-ordinate is negative. This position corresponds to the centre of the optical trap. With the single beam, only one stable equilibrium location (*single beam trap - SBT*) is created. This trap is displaced from the intensity maximum in the direction of the incident beam (see Fig. 3d), which can be attributed to the scattering force. In the

standing wave, there are multiple stable positions (*standing wave traps - SWT's*), which, as illustrated by intensity profile in Fig. 3c, coincide with the GSW antinodes. As no shift of the traps from the intensity maxima is observed, we can conclude that the scattering forces stemming from the two beams (incident and reflected), which create the standing wave, tend to eliminate each other. Consequently, the stability of trapping is improved considerably in comparison with the single beam case.

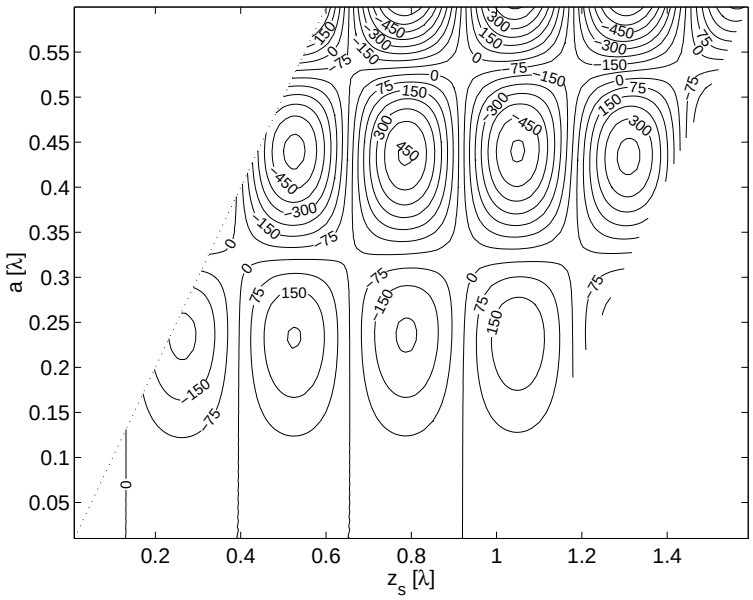

Figure 4. Dependence of the axial trapping force on the position of the particle in the standing wave and the particle size. Numbers at contour lines give the values of the force in pN, dotted line marks the contact of the particle with the reflective surface. Fixed parameters: $w_0 = 1\ \lambda$, $z_0 = 0\ \mu m$, $P = 1W$, $\lambda_{vac} = 1064$ *nm*, $m = 1.19$, $n_{ext} = 1.33$, $\rho = 1$, $\psi = 3\pi/2$.

In the above example, considered particle (diameter 160 nm) was smaller than the spacing of the standing wave antinodes (equal to λ_{vac} / n_{ext}, i.e. 400 nm in our case) so that the particle was influenced by a single antinode. If the particle size is comparable with the standing wave antinode separation, the particle is subject to gradient forces originating from two (or more) neighbouring antinodes. Fig. 4 shows how the axial force depends on the particle radius and the sphere position in the standing wave for polystyrene particles in water. It can be seen that the force does not grow monotonously with increasing particle size. Instead, at a given spatial location z_s, the force oscillates between positive and negative values when the particle radius increases. Because the location of the standing wave nodes and antinodes is fixed relative to the reflective surface, this implies that the particles of growing size are alternately attracted towards the intensity maxima and minima to cover the maximal number of the GSW antinodes and reach the state with minimal energy [19]. There are also particular particle radii, for which the axial force is zero or negative regardless of location of the particle in the standing wave. The

interaction energy of such particles is independent of their position and, therefore, these particles don't "see" the standing wave and cannot be trapped.

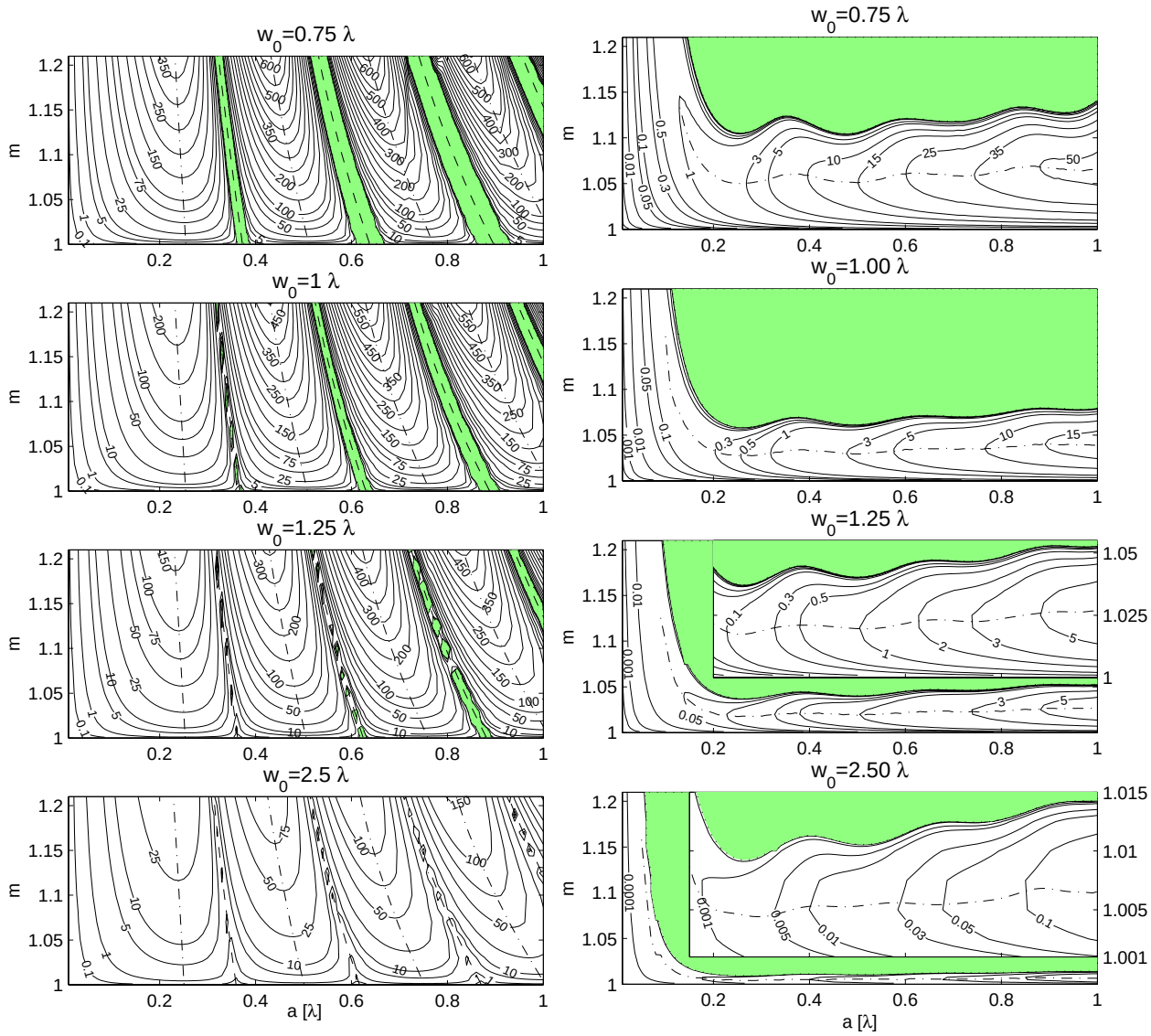

Figure 5. Contour plots of the maximal trapping force (in pN) as the function of the particle size, relative refractive index and beam waist radius in the Gaussian standing wave (left) and single focused beam (right). For beam waist sizes $w_0 = 1.25\lambda$, $w_0 = 2.50\lambda$, the insets in single beam plots show the details of parametric regions, where the stable trapping can be achieved. Dot-and-dashed (dashed) lines represent the curves of maximal (minimal) trapping forces with respect to the particle size. Fixed parameters: $z_0 = 0\ \mu m$, $P=1W$, $\lambda_{vac} = 1064\ nm$, $\rho = 1$, $\psi = 3\pi/2$.

In Fig. 5, the comparison of the optical forces in the standing wave (left) and the single beam (right) arrangements for different particle radii and materials and beam waist sizes is presented. To characterise the trap for a given configuration of the trapping system, the maximal backward axial force F_z^{max} directed (in both cases) against the incident beam propagation is chosen because it is the most critical

parameter, which determines the possibility of stable three-dimensional trapping [15]. Numbers at the contour lines represent levels of constant F_z^{max} in pN. Within the shaded regions, the particle confinement cannot be achieved and the particle is accelerated in the incident beam direction. In the single beam, this is due to a too small axial intensity gradient, which is not sufficient to overcome the scattering forces. In the standing wave, competition of the gradient forces coming from the neighbouring standing wave antinodes, which pull the object in opposite directions and thus cancel each other, plays a leading role. Consequently, weaker gradient force stemming from the focused beam envelope of the Gaussian standing wave dominates and accelerates the particle towards the beam waist placed on the mirror. With the growing beam waist size, the region of relative refractive indices where the object can be confined in the single beam is reduced because the gradient force decreases dramatically (see values of F_z^{max} in contour plots). For bigger particles, the extent of this region further reduces to a close proximity of the unity value of relative refractive index. In the standing wave, the possibility of the stable trapping is given by the particle size and refractive index combination and the beam waist has only a minor influence. On the contrary to the SBT, the size of non-trapping regions decreases for less focused beams. If we compare the values of F_z^{max} in SWT and SBT for bigger particles ($a > 0.5\lambda$), we find that SWT provides maximal trapping forces that are at least an order of magnitude stronger. For smaller particles and wider beam waists (with the exception of the GSW non-trapping regions), this disproportion becomes even more pronounced. When the GSW modulation depth is decreased by using a lower-reflectivity slide or by setting the beam waist location z_0 with respect to the slide to a non-zero value, the dominance of the SWT over the SBT becomes less striking. In practice, most of the trapping experiments actually take place under such conditions. The calculations, however, show that even very small mirror reflectivity of a few % can be sufficient to facilitate the axial confinement of a particle, which still cannot be trapped in the SBT. When operating with the trapping beam focus located close to the mirror ($z_0 = \pm 2\ \lambda$), the standing wave trapping forces can dominate over the single beam ones by an order of magnitude for reflectivity less than 10 %.

Stability of optical trapping

A dielectric particle optically trapped in an immersion medium exhibits stochastic position fluctuations known as the Brownian motion. Kinetic energy of this chaotic thermal motion is the principal effect that influences the stability of optical confinement of small particles. An optically trapped particle moves within a potential well formed by radiation forces together with gravity and buoyancy forces (mechanical forces). The shape of this potential well is given by the properties of the trapped object (size, shape, refractive index, density) and light beam (spatial distribution, total power, direction of propagation with respect to gravity). Generally, its depth is asymmetric in the transversal and axial directions with the latter being the smallest and, therefore, most critical for the stability

of trapping [25]. It is commonly accepted that if the difference ΔW^{tot} between the potential energy of the lowest trap edge and trap bottom is more than $10\ k_BT$ (k_B is the Boltzmann constant and T is the absolute temperature) the particle remains inside the trap for sufficiently long time to be considered confined [11].

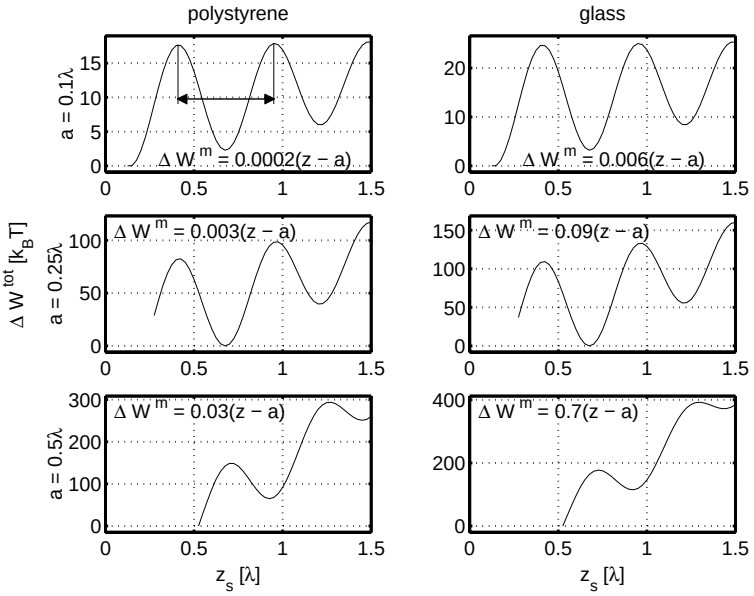

Figure 6. Axial profiles of the potential energy (in k_B T units) in the Gaussian standing wave for polystyrene (m = 1.19) and glass (m = 1.135) particles of different sizes in water. The curves are vertically shifted so that the minimal value of the potential energy is equal to zero in each subplot. Arrow in the upper left subplot indicates the extent of a single standing wave trap. Fixed parameters: P=0.01W, $w_0=0.75\lambda$, $z_0 = 0\ \mu m$, $\lambda_{vac} = 1064$ nm, $\rho = 1$, $\psi = 3\pi/2$.

The axial profile of the trapping potential energy ΔW^{tot} can be found by integrating the total (i.e. optical + mechanical) axial force with respect to the axial co-ordinate. Examples of such potential energy profiles for polystyrene and glass spherical particles trapped in the maximally modulated Gaussian standing wave ($z_0 = 0\ \mu m$, reflectivity 100 %) in water are shown in Fig. 6. In these examples, resulting mechanical force points in the direction of the incident beam. The mechanical part of the total energy ΔW^{m}, however, is negligible in comparison with the total energy ΔW^{tot} as indicated by the slopes of ΔW^{m} with respect to the axial co-ordinate in each subplot. The particle equilibrium positions, which coincide with the local minima of ΔW^{tot}, are thus determined solely by the optical force distributions. It can be noticed that the symmetry of the individual standing wave traps is better for smaller particles, because they do not cover more than one standing wave antinode. For bigger particles, which extend over several antinodes, the effect of the standing wave intensity oscillations is averaged and the single focused beam envelope is thus more pronounced. When the particle size increases ($a = 0.25\lambda \rightarrow a = 0.5\lambda$), the particle equilibrium positions shift from the GSW antinodes to nodes, as already demonstrated in Fig. 4.

The knowledge of the axial potential energy profile can be used to obtain minimal trapping power P^{min} that is necessary for stable axial confinement of a particle. This value is given by the laser power, for which the trap depth is equal to $10\ k_BT$ (see also Fig. 6). The comparison of P^{min} needed in the Gaussian standing wave and single focused beam shows that the difference is not as big as the difference in the corresponding maximal trapping forces. This can be explained by the fact that the trap depth, unlike the trapping force, is not proportional to the intensity gradient but rather to the difference between the global intensity maximum and minimum. Therefore, the spatial intensity distribution is not so important in this case.

Standing wave trap stiffness

The stiffness of an optical trap characterises the restoring force acting on a trapped particle, which is displaced from its equilibrium position in the trap. It is defined as the derivative of the force with respect to the spatial co-ordinate in the direction of the displacement, evaluated at the equilibrium position (see Fig. 7).

Generally, the stiffness is a function of the displacement. If, however, the trapping potential is assumed to be harmonic (which can be done for sufficiently small deviations of the trapped particle from its equilibrium position [9]), the stiffness is fully determined by a single constant. Consequently, the restoring force is directly proportional to the displacement. In Fig. 7, the examples of the axial force profiles of the standing wave (a) and single beam (b) traps are shown together with their equilibrium position tangents, which make an angle α with the z co-ordinate. The slopes of these tangents (proportional to $tan\alpha$) define, in the first order approximation, the trap stiffness. The accuracy of this approximation can be estimated by looking at the profiles of ΔW^{tot} of both traps (c), (d) and their departure from harmonic behaviour. As a stable trapped particle is spatially confined to the region, where the change of the potential energy with respect to the equilibrium position does not exceed the value of $10\ k_BT$, it is sufficient to analyse only the potential energy changes below this level. In the standing wave case (c), there is a negligible difference between the actual value of ΔW^{tot} and the parabolic fit within the range of interest (maximal relative error is less than 5 %). The harmonic approximation is fulfilled well and the trap stiffness within the region explored by the trapped particle is thus constant. On the other hand, single beam potential energy profile for the same beam waist radius and total beam power (d) shows significant departures from the parabola already at energies of $\sim 2\ k_BT$. Moreover, the potential well is asymmetric in the axial direction. This can be attributed to the scattering forces, which shift the trapped particle out of the beam focus in the incident beam direction (see Fig. 3). As a result, the linearity of the SBT in the axial direction is significantly worse than for the SWT case. To improve the SBT performance, it is necessary to increase the trapping beam power, which leads to a directly proportional deepening of the trap and restriction of the particle movement to a closer proximity of the equilibrium position. The calculation of the axial trap stiffness for the GSW and single focused beam reveals that the stiffness, which can

be achieved in the SWT is at least two orders of magnitude bigger [16]. This conclusion implies much more precise axial confinement of a particle in the SWT than in the SBT for the same beam waist radius and total beam power.

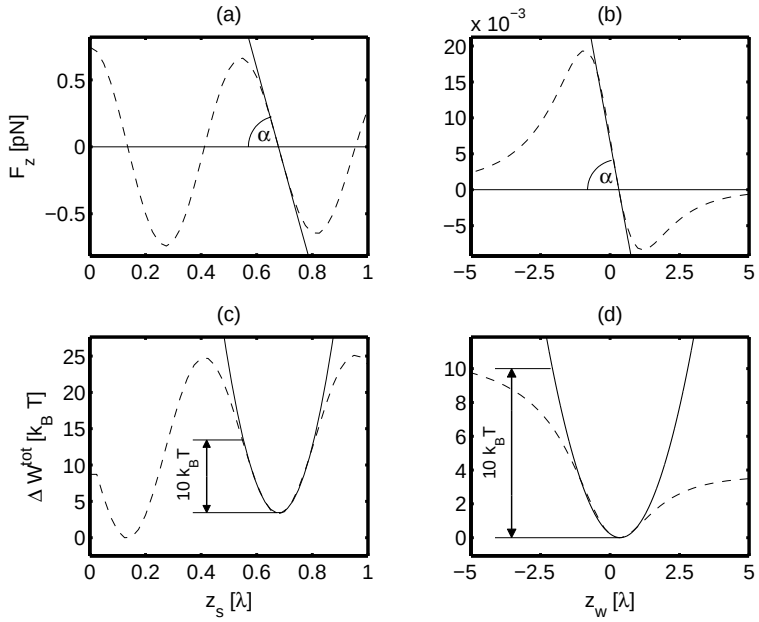

Figure 7. Definition of the standing wave and single beam trap stiffness. In the top row, standing wave force plotted against the distance z_s of the particle from the reflective surface (a) and single beam force plotted against the distance z_w of the particle from the beam waist (b) are shown (dashed lines). Solid straight lines represent the tangents to the force profiles at the particle equilibrium positions. In the bottom row, corresponding profiles of the trapping potential energy ((c), (d) - dashed lines) are presented together with their parabolic fits (solid lines). Fixed parameters: $a = 0.1\lambda = 80$ nm, $m = 1.19$, $w_0 = 0.75\lambda$, $z_0 = 0$ μm, $P = 0.01$ W, $\lambda_{vac} = 1064$ nm, $\rho = 1$, $\psi = 3\pi/2$.

3.3 Practical realisation of the standing wave trap

3.3.1 Experimental set-up for the optical confinement and micromanipulation

An optical trap, which uses the interference-created standing wave for the confinement of dielectric particles of radii ranging from tens of nanometers to tens of micrometers can be built up using the same principal components that constitute the classical single beam optical tweezers [9,17]. The only difference between the two trapping techniques is the introduction of a specially coated slide, which displays very high reflectivity for the chosen trapping wavelength, as the boundary of the trapping cell in the standing wave set-up.

A schematic drawing of the experimental set-up is shown in Fig. 8. Whole system was built around an inverted optical microscope. A Nd:YVO_4 laser (λ_{vac} = 1064 nm, P_{max} = 2 W at TEM_{00} mode) served as the source of the trapping light. Another fundamental component of the trapping system is a high numerical aperture objective lens, which focuses down the laser beam to create necessary gradients of the optical intensity and which also facilitates the observation of the manipulated

specimen. In the presented measurements, Plan-Neofluar 100x, N.A. = 1.3, oil immersion lens (Carl Zeiss) was used. Vertical position of the objective and, thus, also the position of the trap relative to the sample chamber walls could be fine-adjusted by a piezoactuator attached to the objective mount and controlled by a computer.

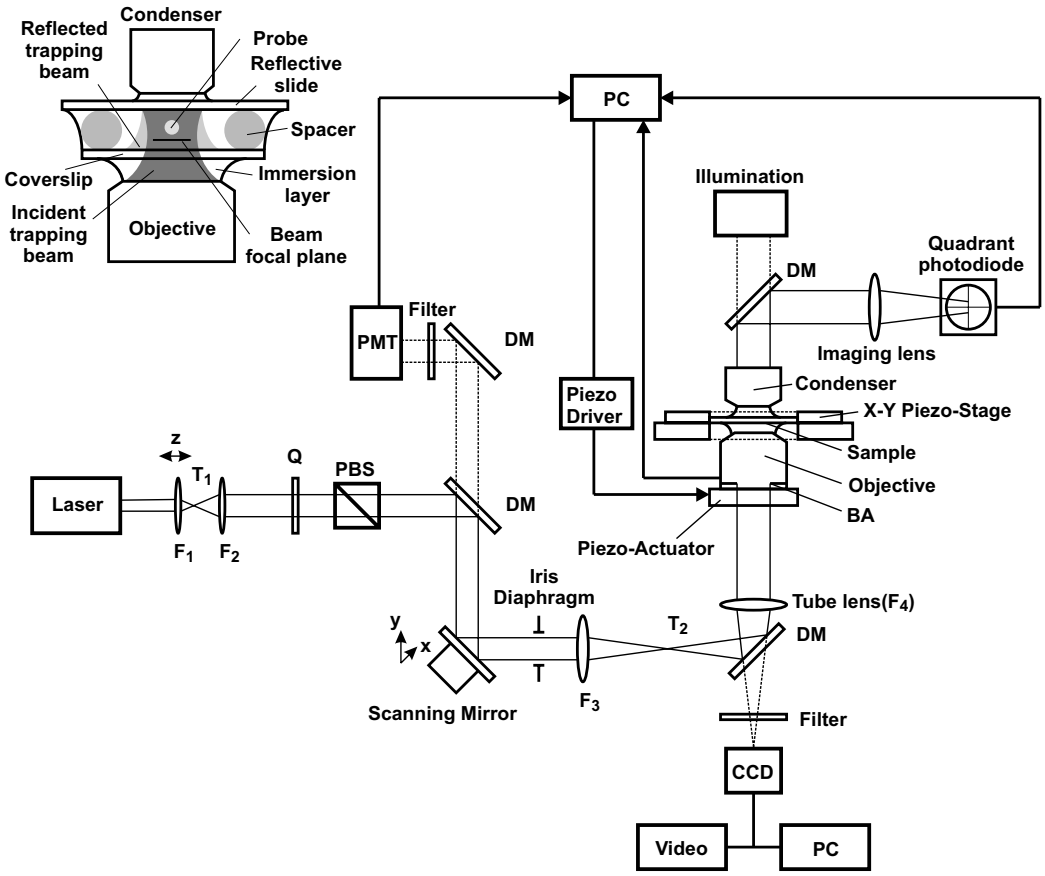

Figure 8. Experimental set-up used for the comparative study of the standing wave and single beam trapping. Legend: Q - half-wave retardation plate, PBS - polarising beam splitter, DM - dichroic mirrors, T_1 - T_2 - telescopes, BA - objective back aperture, PMT - photomultiplier tube. In the top left corner, a detail of the sample chamber is shown.

Before entering the objective, the laser beam passed through an additional optical system, which enabled to gain control over the position of the trap in the microscope's field of view and it also magnified the beam diameter to slightly overfill the objective back aperture and fully exploit its numerical aperture. The lenses were arranged in such a way that the beam width at the objective back aperture did not change during the trap positioning [14]. The power transmitted through the objective was thus the same regardless the trap position and the trap quality was not degraded. The trapping particles (probes) were placed in a sealed chamber constituted by a specially coated slide and an ordinary glass coverslip separated by suitable spacers (see detail in Fig. 8). Inside the sample chamber, the focused trapping beam was back reflected from the coated slide to create the standing wave. To facilitate the sample observation, the reflective slide was

transparent for the visible light. The whole manipulated sample was placed into the X-Y piezo-driven stage mounted on an ordinary mechanical microscope stage, which enabled fine positioning (with nanometer precision) of the sample. The experiment could be monitored on-screen by a CCD camera, which also enabled to record images either to videotape or to PC.

3.3.2 Measurement of the optical trap stiffness

For small displacements of the trapped particle from its equilibrium position, the trap stiffness in a particular direction is given by a single constant and the trapping force is directly proportional to the particle displacement. This implies that the knowledge of the trap stiffness facilitates experimental measurement of the optical forces via detection of the trapped particle position [9]. To detect the particle position in our set-up, the trapping light, which had passed through the sample chamber was collected by an oil-immersion condenser with N.A. = 1.4, and projected onto the surface of a quadrant photodiode. The adopted detection scheme makes use of the interference pattern of the light scattered from the object and unscattered incident light, whose changes are detected at the plane optically conjugated with the condenser back focal plane. Here, the axial particle shifts manifest themselves as the fluctuations of the total intensity intercepted by the detector. In the transversal direction, the detector signal arises from breaking the rotational symmetry between the two interfering fields when the particle is located off-axis and it is obtained from the difference of intensities measured by the left and right (or the top and bottom) halves of the detector [26].

There are several experimental methods, which enable to determine the trap stiffness [9]. Most frequently, they make use of the thermal position fluctuations of the trapped particle. For a known viscous drag coefficient β of the particle, calculation of the power spectral density (PSD) of the trapped object position can provide desired information [27]. It takes, for a harmonically bound particle in a viscous environment at low Reynolds numbers, the form:

$$S_z(f) = \frac{k_B T}{\beta \pi^2 (f^2 + f_C^2)}. \tag{3.1}$$

Here, $S_z(f)$ is the PSD of the axial position signal and $f_C = \kappa / (2\pi\beta)$ is the characteristic (corner) frequency of the spectrum. The trap stiffness can be determined from the corner frequency by fitting the power spectrum (3.1) to a Lorentzian. Because the value of f_C is independent of the actual magnitude of the particle position fluctuations, the position detector calibration is not necessary. An alternative to this method is the use of the autocorrelation function (ACF) $\langle z(0)z(t)t \rangle$ of the position signal instead of PSD. According to the Wiener-Khinchin theorem, these two functions form a Fourier-transform pair [28], i.e.

$$\langle z(0)z(t)\rangle = FT(S_z(f)) = \langle \Delta z^2 \rangle \exp\left(-\frac{\kappa}{\beta}t\right), \tag{3.2}$$

and the requirements and advantages of both approaches are essentially identical.

A different approach uses the Boltzmann statistics to map the potential energy profile, and, thus, also the trap stiffness. This method in principle overcomes the restriction to harmonic potentials and requires only the knowledge of the fluid's temperature [29]. Therefore, it enables to measure other parameters, such as the particle drag coefficient, by combining it with the previously mentioned method [30]. Boltzmann statistics

$$p(z) = C\exp\left(-\frac{\Delta W^{tot}(z)}{k_B T}\right), \tag{3.3}$$

where C is a normalisation constant, describes the probability $p(z)dz$ of finding a particle in an infinitesimal interval dz around the location z in thermal equilibrium. If this probability density $p(z)$ is measured, which can be done by making the histogram of the recorded position fluctuations Δz over a sufficiently long time period, the potential experienced by the particle can be calculated as

$$\Delta W^{tot}(z) = -k_B T \ln p(z) + k_B T \ln C. \tag{3.4}$$

The last term determines the potential offset and can be neglected. By fitting a parabola to the potential profile (3.4), the trap stiffness is easily calculated.

From the theoretical analysis, it follows that the strength and stiffness of the classical single beam optical trap is several times higher in the transversal direction than in the axial one [15,31]. This is a direct consequence of unequal steepnes of the respective intensity gradients (compare with Fig. 2). On the other hand, this disproportion in the standing wave should be reduced or - for a moderately focused beam - even reversed. This is due to the significant growth (by orders of magnitude) of the SWT axial stiffness in comparison with the single beam arrangement for the same trapping beam parameters (beam waist radius, total power) while the transversal stiffness increase keeps below the factor of 4 [16]. To verify this, the axial and transversal trap stiffnesses were measured using standing wave generating slides of different reflectivity and also without the presence of a reflective slide. For the standing wave trapping, the particles were placed in a chamber, which consisted of a coverslip at the objective side and a coated slide reflecting the incident beam at the condenser side (see detail in Fig. 8). The distance between the slide and the coverslip was set by spacer latex beads with a nominal diameter of *21.4 μm*. The chamber was sealed by silicon grease, which proved to be sufficient to maintain constant separation distance between the two glasses during the experiment. For the single beam trap study, the reflective slide was replaced with another ordinary

coverslip and the distance between the two coverslips was increased to 1.22 mm in order to exclude any back-reflection effects.

The stiffness measurements were carried out with polystyrene beads ($a = 108$ *nm*, $m = 1.19$), which were dispersed in deionized water in sufficiently low concentration to prevent multiple beads from entering the trap simultaneously. Measured position signals were sampled by a data acquisition board, stored in computer memory and off-line processed using IgorPro software package (WaveMetrics). For the standing wave set-up, performance of the trap for two slide reflectivities (R = 54 % and R = 98.5 %) and several distances of the beam focus from the slide was analysed. The experiments for each slide were performed for two different laser beam focusations, which were adjusted using an iris diaphragm placed in the optical path in front of the microscope (see Fig. 8). The trapped particle was always located in the vicinity of the trapping beam focus. The single beam measurements were done nearby the objective-side coverslip to minimise the influence of the objective spherical aberration on the trap performance [29]. From the sampled detector signals, uncalibrated position histograms (probability densities - Eq. (3.3)), and autocorrelation functions (Eq. (3.2)) were calculated using standard numerical algorithms [32]. The knowledge of two independent features of the measured data sets then gave an opportunity of simultaneous determination of two unknown parameters of the trapping system [30]. Consequently, it was possible to do *in situ* calibration of the position detector, and, at the same time, determine the trap stiffness with the assumption of known drag coefficient of the spherical particle $\beta = 6\pi\eta$, where the water viscosity η at the laboratory temperature $T = 298^{o}\ K$ and particle radius a were set to values $\eta = 0.8 \times 10^{-3}\ Pa.s$ and $a = 108\ nm$, respectively. The detector calibration constant and trap stiffness κ were determined from an exponential fit to the ACF and a parabolic fit to the potential profile, respectively.

The summary of the stiffness measurement is presented in Tab. 1, 2, and 3. For each reflectivity R and distance z_0 of the beam focus from the reflective slide (SWT) or $z_{coverslip}$ of the beam focus from the objective-side coverslip (SBT), the measurement of the transversal stiffnesses κ_x, κ_y and the axial stiffness κ_z was repeated 5-9 times with different beads captured out of solution. Because the trap stiffness is directly proportional to the laser power, all values were re-calculated to the same nominal value of power $P = 1W$. However, direct comparison of the stiffness values was only possible for the SBT and the SWT with the fully open iris diaphragm as for the SWT with iris closed to diameter 1.5 mm (objective back aperture diameter was 5 mm), the ratio of the power transmitted through the objective to the power at the objective BA is different. The most useful parameter for the trap comparison, therefore, is the ratio of the transversal-to-axial trap stiffness, which is independent of power and objective transmission factor. It can be seen in Tab. 1 that for the SBT, the transversal stiffness is generally several times higher than the axial one. A slight asymmetry in the x and y directions is due to the effect of the light polarisation direction.

$z_{coverslip}$ [μm]	κ_x [10^{-5} N.m^{-1}]	κ_y [10^{-5} N.m^{-1}]	κ_z [10^{-5} N.m^{-1}]	κ_x/κ_z	κ_y/κ_z
3.94 ± 0.26	3.93 ± 0.23	4.83 ± 0.95	0.78 ± 0.06	5.03	6.19

Table 1. Measured average SBT stiffness and stiffness standard deviation for a = 108 nm polystyrene beads re-calculated to the nominal power of 1 W at the objective back aperture. $z_{coverslip}$ gives the distance of the trapping beam focus from the objective-side coverslip. Stiffness values were determined from five successive measurements.

In the SWT with the same focal spot size (Tab. 2), however, the ratio of the transversal-to-axial stiffness is improved by the factor of 3 to 5. For a constant slide reflectivity, the improvement is more significant if the trapped particle is situated closer to the slide. The decrease of the absolute values of κ_x, κ_y in the SWT is due to the spherical aberrations - particles in the SWT were trapped farther from the objective side coverslip than in SBT (more than 10 μm vs. 4 μm), which degraded the trapping beam.

R [%]	z_0 [μm]	κ_x [10^{-5} N.m^{-1}]	κ_y [10^{-5} N.m^{-1}]	κ_z [10^{-5} N.m^{-1}]	κ_x/κ_z	κ_y/κ_z
54	4.25±0.19	2.52±0.43	3.38±0.59	2.73±0.61	0.92	1.24
54	10.99±0.33	2.13±0.37	2.81±0.47	1.25±0.29	1.70	2.25
98	9.24±0.10	2.12±0.30	2.55±0.32	1.38±0.25	1.54	1.85

Table 2. Measured average SWT stiffness and stiffness standard deviation for a = 108 nm polystyrene beads with fully exploited objective lens N.A. re-calculated to the nominal power of 1 W at the objective back aperture. z_0 gives the distance of the trapping beam focus from the reflective slide. Stiffness values were determined from nine successive measurements.

If the focal spot size is increased by closing down the iris diaphragm, the axial trap stiffness dominates over the transversal one as illustrated in Tab. 3. Higher slide reflectivity and smaller distance from the reflective slide support the effect. The maximal observed increase in transversal-to-axial stiffness ratio in the presented comparison of the SBT and SWT was the factor of 13.

R [%]	z_0 [μm]	κ_x [10^{-5} N.m^{-1}]	κ_y [10^{-5} N.m^{-1}]	κ_z [10^{-5} N.m^{-1}]	κ_x/κ_z	κ_y/κ_z
54	4.25±0.19	4.14±0.22	5.84±0.26	10.61±2.42	0.39	0.55
54	10.99±0.33	3.64±0.20	4.10±0.35	5.40±0.60	0.67	0.76
98	9.24±0.10	4.14±0.18	5.39±0.56	8.85±0.90	0.47	0.61

Table 3. Measured average SWT stiffness and stiffness standard deviation for a = 108 nm polystyrene beads with reduced objective lens N.A. re-calculated to the nominal power of 1 W at the objective back aperture. z_0 gives the distance of the trapping beam focus from the reflective slide. Stiffness values were determined from nine successive measurements.

Trap type	$(\kappa_x/\kappa_z)_{th}$	$(\kappa_x/\kappa_z)_{exp}$	$(\kappa_y/\kappa_z)_{th}$	$(\kappa_y/\kappa_z)_{exp}$
SBT ($z_{coverslip}$ = 3.94 μm)	4.21	5.03	5.80	6.19
SWT (R = 54 %, z_0 = 4.25 μm)	0.25	0.92	0.34	1.24
SWT (R = 54 %, z_0 = 10.99 μm)	0.51	1.70	0.72	2.25
SWT (R = 98 %, z_0 = 9.24 μm)	0.60	1.54	0.80	1.85

Table 4. Comparison of theoretically and experimentally determined transversal-to-axial trap stiffness ratios in the single beam and standing wave traps. Theoretical data were obtained from the GLMT calculation, which uses fifth-order corrected Gaussian beam formulas for description of the field incident upon the trapped particle.

To compare measured ratios of transversal-to-axial trap stiffness with theoretical predictions, trap stiffnesses for the combinations of parameters z_0, w_0, a, m and R corresponding to experimental values were calculated using GLMT formalism. The calculation results are presented along with the measured data in Tab. 4. It can be seen that the agreement between the theory and experiment is reasonably good for the single beam trap (the relative difference $(ratio_{exp} - ratio_{th}) / ratio_{th}$ between both values is below 20 %). On the other hand, the calculated and measured values of the transversal-to-axial trap stiffness ratios in the standing wave differ much more with the relative difference varying between 131 % and 268 % for the studied cases. This discrepancy can be attributed to the departure of the actual field incident upon the particle from the idealised Gaussian standing wave used in the model.

Trap type	$(\kappa_x/\kappa_y)_{th}$	$(\kappa_x/\kappa_y)_{exp}$
SBT ($z_{coverslip}$ = 3.94 μm)	0.73	0.81
SWT (R = 54 %, z_0 = 4.25 μm)	0.74	0.74
SWT (R = 54 %, z_0 = 10.99 μm)	0.71	0.76
SWT (R = 98 %, z_0 = 9.24 μm)	0.75	0.83

Table 5. Comparison of theoretically and experimentally determined ratios of the transversal trap stiffnesses in the predominate polarisation direction (x-axis) and direction perpendicular to it (y-axis) for the single beam and standing wave traps.

Tab. 5 reveals that, although the theory is not fully successful in describing the realistic relation between the transversal and axial trap stiffnesses, it gives a very good prediction of the trap asymmetry in two perpendicular transversal directions defined relative to the orientation of the predominant polarisation of the incident wave. In this case, the relative difference between theory and measurement does not exceed 11 %.

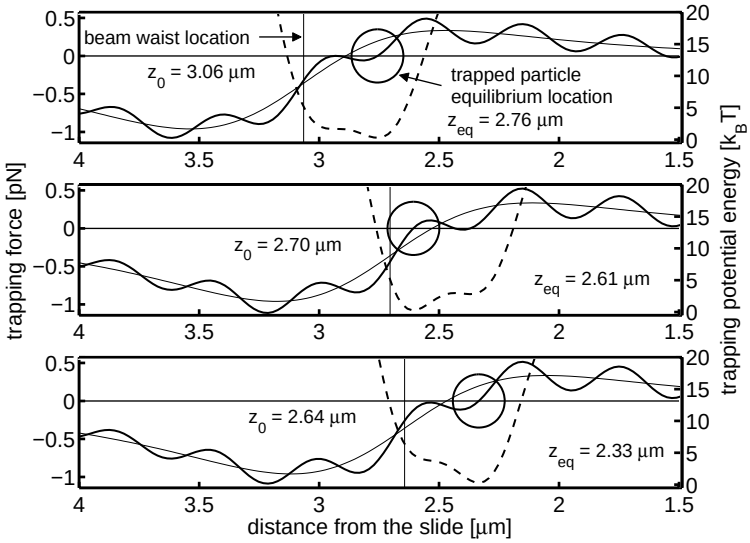

Figure 9. Theoretical profiles of the trapping force (thick solid lines) and trapping potential energy (dashed lines) of the single beam trap modulated by the reflection from a glass - water interface at different distances z_0 of the beam focus from reflective surface. The trapped particle is located at z_{eq} (places of zero force and potential minima). Diameter of circles corresponds to the actual probe size (a = 108 nm) used in simulations and experiments. The other parameters are: R = 0.4 %, w_0 = 0.475 μm, P = 80 mW. Under these conditions, average contribution of the standing wave component to the total intensity is less than 3 %. For comparison, thin solid lines show the pure single beam trap force profile (i.e. without reflection) for the same parameters.

3.3.3 Coexistence of the single beam and standing wave trapping

Whenever a reflected wave is generated, the trapped particle is subject to combined forces originating both from the axial optical intensity gradients of the focused beam envelope and the gradients in the spatially oscillating field. In Fig. 9, theoretical GLMT-based simulations of the axial trapping force and trapping potential energy are shown, for the case of trapping in the beam modulated by the reflection from a glass - water interface with reflectivity of approximately 0.4 %. The simulations demonstrate that the distance of the trapped particle from the focus of the standing wave modulated beam changes when the focus is moved towards the slide (top to bottom subplots). This differs from the case of trapping with an unmodulated beam, where the probe follows the motion of the beam focus (see thin solid lines in Fig. 9).

The above-described behaviour can be visualised by monitoring the intensity of the fluorescence, which is excited by the two-photon absorption of the trapping light in the fluorescently labelled-trapped particle [33]. The procedure uses the fact that the intensity of fluorescence (two-photon signal - TPS) emitted from the trapped particle is proportional to the square of the local optical intensity and, thus, changes with axial displacement of the particle with respect to the beam focus. With this method, nanometer resolution in position sensing can be achieved. To measure the

intensity of the TPS, the trapping set-up was completed with a photomultiplier tube connected to a photon counting unit and a computer with data acquisition board (see Fig. 8).

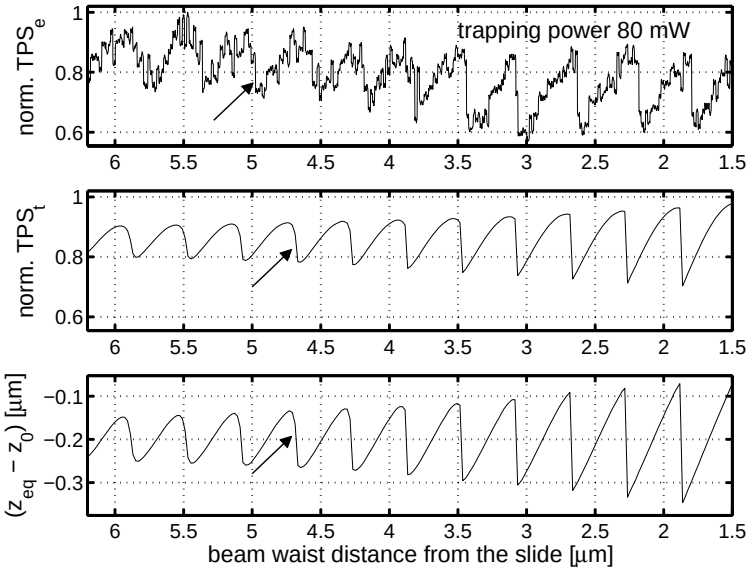

Figure 10. Comparison of experimentally recorded TPS (top) with theoretical simulation (middle) for the case of reflection from a glass - water interface. The simulation parameters are identical to those used in Fig. 11 and correspond to experimental conditions. The bottom subplot shows calculated distance of the trapped particle from the beam focus. To visualise clearly the detailed features of signals, only a narrow interval of beam-waist-to-slide distances is displayed. Arrows indicate the transition between smooth modulation of the particle position and abrupt jumps.

Experimentally obtained results recorded during pushing the trapped probe towards a glass slide placed in water are presented together with theoretical simulations in Fig. 10. The trap movement was achieved using the piezoactuator-mounted objective lens, and the TPS was recorded synchronously with the actual trap position. The normalised measured TPS plotted against the distance of the beam waist from the reflecting slide is shown in the top subplot. Sawtoothlike structure of the signal is a consequence of shifts of the trapped probe equilibrium position in the standing wave modulated optical field (see Fig. 9). While approaching the slide, the standing wave modulation depth increases with increasing ratio of the amplitudes of divergent reflected and incident beam. The influence of the standing wave on the total trapping force thus increases and the smooth modulation of the particle equilibrium position turns to abrupt jumps between successive equilibrium positions. This transition indicates the dominance of standing wave trapping over single beam trapping and can be distinguished approximately at the distance of 5 µm from the slide. In the middle subplot, a theoretical simulation of the TPS is shown. Theoretical values of the TPS were determined by integrating the square of the local optical intensity at the equilibrium position over the particle volume, assuming a homogeneous distribution of the dye within the particle. Despite an idealised description of the incident wave (Gaussian beam), the coincidence of the measured

and calculated TPS is very good. The comparison between the middle and bottom subplots of Fig. 10 reveals clearly the correlation between the TPS value and particle - beam waist distance.

When the slide reflectivity is increased, the extent of the standing wave dominance region grows and the single beam trapping can eventually be completely suppressed. This means the particle can get confined at a fixed position in the standing wave and stop following the beam waist movement at all.

4 CONCLUSION

The transfer of momentum between the focused laser light and material bodies has been investigated in a number of experiments during the past thirty years. It has been proved that the light beam with appropriate intensity distribution, which features strong intensity gradients, can serve to confine in three dimensions micron and submicron-sized dielectric particles surrounded by an optically less dense medium. The present applications of the optical trapping cover a wide range of research activities in the fields of life and material sciences, e.g. the study of the mechanical properties of single cells and even single biological macromolecules (viscoelasticity, fluidity), measurement of the forces exerted by tiny molecular motors, which power the cell motion, and the construction of new types of the subwavelength-resolution microscopes.

The most frequently used experimental arrangement for the optical trapping - optical tweezers - achieves the necessary intensity gradients by a tight focusing of a single laser beam with a high quality microscope objective. This set-up, however, suffers from the asymmetry of the trap, which is several times weaker along the incident beam direction than in the transversal direction. Recently, a novel method of the intensity gradient generation was proposed at the author's home laboratory, which uses the interference of the two counter-propagating coherent waves to create spatially oscillating standing wave with the Gaussian transversal profile. One of the two waves is then generated by retro-reflection of the incident beam from a planar surface. The axial optical forces, which arise here due to the steep intensity changes between the standing wave minima and maxima, can be by several orders of magnitude higher than those provided by the classical set-up. The stability of the trapping is thus considerably improved. Moreover, the repeating intensity pattern enables to confine several objects simultaneously.

In this Ph.D. thesis, I have analysed the features of this novel type of optical trap both theoretically and experimentally. I have derived formulas, which give the optical forces acting on a spherical dielectric particle in a Gaussian standing wave, and I have developed the software which enables to calculate the standing wave optical forces for various parameters of the trapping system (particle size and refractive index, laser beam waist size and distance of the waist from the reflective surface, surface reflectivity) as well as other characteristics of the optical trap (depth, stiffness). By comparison with the corresponding characteristics of the classical single beam trap calculated for the same parameters, our research team has

then proved the superiority of the standing wave based scheme in that it provides stronger forces and stiffer, deeper trap, especially in the axial direction.

The experimental part of this work was aimed at the practical realisation of the standing wave trapping system and verification of theoretically predicted conclusions. Applying the standing-wave-generating slides of different reflectivity, I have measured the ratio of the transversal-to-axial trap stiffness. This measurement has proved that the mentioned stiffness ratio in the standing wave increases with respect to the single beam trapping in agreement with the simulation and this increase is more significant if a less focused beam is used. Using a fluorescently labelled-trapped probe, I studied the coexistence of the standing wave and single beam trapping modes. Notable influence of the standing wave on the trapping was observed even in the close proximity of an ordinary glass - water interface. As this effect is usually not taken into account, it leads to artefacts, for example, in the measurement of the surface potential profiles. We have also experimentally demonstrated the possibility of the simultaneous manipulation of several dielectric objects on polystyrene particles of sizes ranging from subwavelength region to several wavelengths and on yeast cells. A potential application of this feature of the standing wave trap could be, for example, preparation of crystal-like structures constituted by colloidal particles.

In summary, the presented Ph.D. thesis is, up to my knowledge, the first work, which synthesises detailed theoretical and experimental investigation of the optical trapping in the interference-generated standing wave. Although the theory, which uses an idealised description of the incident electromagnetic field, is not fully successful in exact quantitative description of a real trapping system suffering from various aberrations, it provides important information about general trends, which can be expected when the trapping system parameters are changed. The experiments then confirm superior stability of the standing-wave-based optical trap over the conventionally used single beam system and reveal the presence of the standing wave component of the total field in the vicinity of virtually any surface of the refractive index discontinuity.

5 ZÁVĚR

Přenos hybnosti mezi fokusovaným světlem laseru a hmotnými objekty byl v uplynulých třiceti letech studován v řadě experimentů. Bylo prokázáno, že světelný svazek s vhodným rozložením intenzity, které se vyznačuje přítomností silných intenzitních gradientů, může sloužit k prostorovému zachycení objektů mikrometrových a submikrometrových rozměrů obklopených opticky řidším prostředím. Současné aplikace optického chytání pokrývají široké spektrum výzkumných aktivit v oblasti věd o živé i neživé přírodě. Mezi nejvýznamnější patří například studium mechanických vlastností (viskoelasticita, fluidita) jednotlivých buněk a dokonce jednotlivých biologických makromolekul, měření sil vyvolaných molekulárními motory, které umožňují pohyb buněk a konstrukce nových typů mikroskopů využívajících zachycenou částici jako lokální sondu.

V nejčastěji využívaném experimentálním uspořádání pro optické mikromanipulace - optické pinzetě - je nezbytných gradientů intenzity dosaženo silnou fokusací jediného laserového svazku pomocí kvalitního mikroskopového objektivu. Takto vytvořená optická past je ovšem nesymetrická a síly, působící v osovém směru, jsou několikrát menší než příčné síly. Nedávno byla v domovské laboratoři autora navržena nová metoda, která využívá k vytvoření gradientu intenzity interference dvou protiběžných koherentních vln, z nichž jedna je generována odrazem dopadajícího svazku od rovinného rozhraní. Superpozicí těchto vln vzniká stojatá vlna s gaussovským příčným profilem a oscilujícím osovým profilem intenzity. Osové síly, které zde vznikají v důsledku prudkých změn intenzity mezi uzly a kmitnami stojaté vlny, mohou být až o několik řádů větší, než síly v klasickém uspořádání. Stabilita zachycení je tudíž výrazně vyšší. Kromě toho umožňuje periodický profil intenzity simultánní zachycení několika objektů.

V disertační práci jsem teoreticky a experimentálně analyzoval vlastnosti tohoto nového typu optické pasti. Odvodil jsem výrazy, které udávají optické síly působící na kulovou dieletrickou částici v gaussovské stojaté vlně a vyvinul jsem počítačový program umožňující výpočet sil a dalších charakteristik optické pasti ve stojaté vlně (hloubka pasti, tuhost) pro různé parametry chytacího systému (velikost a relativní index lomu kuličky, rozměr pasu svazku a vzdálenost pasu svazku od odrazné plochy, odrazivost plochy). Srovnáním s korespondujícími charakteristikami klasické jednosvazkové optické pasti vypočítanými pro totožné parametry chytacího systému prokázal náš výzkumný tým přednosti využití stojaté vlny v tom, že umožňuje dosažení větších sil, hloubky a tuhosti pasti zejména v osovém směru.

Experimentální část práce byla zaměřena na praktickou realizaci systému pro manipulace ve stojaté vlně a ověření teoreticky předpovězených závěrů. Pro několik různě odrazných skel vytvářejících stojatou vlnu jsem změřil poměr osové a příčné tuhosti optické pasti obsahující zachycenou částici o rozměru stovek nanometrů. Toto měření potvrdilo, že poměr tuhostí ve stojaté vlně je vyšší než v jednosvazkovém uspořádání a - v souladu se simulací - je nárůst tohoto poměru výraznější pro méně fokusované svazky. S využitím fluorescenčně značené zachycené sondy jsem studoval koexistenci optického chytání ve stojaté vlně a fokusovaném svazku. Dokonce i v blízkosti rozhraní voda - sklo byl pozorován výrazný vliv stojaté vlny na chytání. Jelikož tento vliv není obvykle brán v úvahu, může například vést k artefaktům při měření profilů povrchového potenciálu. Na polystyrenových kuličkách nanometrových a mikrometrových rozměrů a na kvasinkách jsme demonstrovali možnost simultánní manipulace s několika dielektrickými objekty. Potenciální aplikace této vlastnosti optické pasti ve stojaté vlně může být například v oblasti přípravy krystalických struktur složených z koloidních částic.

Podle mého vědomí je tato disertační práce první systematickou studií, která spojuje teoretické i experimentální aspekty optického chytání ve stojaté vlně vytvořené interferencí. Ačkoli teorie, která používá idealizovaný popis dopadajícího elektromagnetického pole, není stoprocentně úspěšná v přesném kvantitativním

popisu reálného chytacího systému zatíženého různými aberacemi, poskytuje důležité informace o obecných trendech, které mohou být očekávány při změně parametrů chytacího systému. Experimenty pak potvrzují lepší stabilitu optické pasti ve stojaté vlně ve srovnání s jednosvazkovým uspořádáním a ukazují přítomnost stojaté vlny ve výsledném elektromagnetickém poli v blízkosti libovolného rozhraní prostředí s různým indexem lomu.

6 REFERENCES

[1] Ashkin, A. Acceleration and trapping of particles by radiation pressure. *Phys. Rev. Lett.* 1970, vol. 24, p. 156-159.

[2] Block, S. M., Blair, D. F., Berg H. C. Compliance of bacterial flagella measured with optical tweezers. *Nature* 1989, vol. 338, p. 514-518.

[3] Block, S. M., Goldstein, L. S. B., Schnapp, B. J. Bead movement by single kinesin molecules studied with optical tweezers. *Nature* 1990, vol. 348, p. 348-352.

[4] Svoboda, K., Schmidt, C. F., Schnapp, B. J., Block, S. M. Direct observation of kinesin stepping by optical trapping interferometry. *Nature* 1993, vol. 365, p. 721-727.

[5] Walz, J. Y., Prieve, D. C. Prediction and measurement of the optical trapping forces on a microscopic dielectric sphere. *Langmuir* 1992, vol. 8, p. 3073-3082.

[6] Ghislain, L. P., Webb, W. W. Scanning-force microscope based on an optical trap. *Opt. Lett.* 1993, vol. 18, p. 1678-1680.

[7] Sasaki, K., Fujiwara, H., Masuhara, H. Optical manipulation of lasing microparticle and its application to near-field microspectroscopy. *J. Vac. Sci. Technol. B* 1997, vol. 15, p. 2786-2790.

[8] Masuhara, H., Schryver, F. C. D., Kitamura, N., Tamai, N. *Microchemistry.* Spectroscopy and Chemistry in small domains. 1st ed. Amsterdam: Elsevier, 1994. 571 p. Delta Series. ISBN 0-444-81513-9

[9] Svoboda, K., Block, S. M. Biological applications of optical tweezers. *Ann. Rev. Biophys. Biomol. Struct.* 1994, vol. 23, p. 247-285.

[10] Stratton, J. A. *Teorie elektromagnetického pole.* Praha: SNTL, 1961.

[11] Ashkin, A., Dziedzic, J. M., Bjorkholm, J. E., Chu, S. Observation of a single-beam gradient force optical trap for dielectric particles. *Opt. Lett.* 1986, vol. 11, p. 288-290.

[12] Sato, S., Ishigure, M. Optical trapping and rotational manipulation of microscopic particles and biological cells using higher-order mode Nd:YAG laser beams. *Electron. Lett.* 1991, vol. 27, p. 1831-1832 .

[13] Taguchi, K., Ueno, H., Hiramatsu, T., Ikeda, M. Optical trapping of dielectric particle and biological cell using optical fibre. *Electron.Lett.* 1997, vol. 33, p. 413-414.

[14] Fallman, E., Axner, O. Design for fully steerable dual-trap optical tweezers. *Appl. Opt.* 1997, vol. 36, p. 2107-2113.

[15] Ashkin, A. Forces of a single-beam gradient laser trap on a dielectric sphere in the ray optics regime. *Biophys. J.* 1992, vol. 61, p. 569-582.

[16] Zemánek, P., Jonáš, A., Šrámek, L., Liška, M. Optical trapping of Rayleigh particles using a Gaussian standing wave. *Opt. Commun.* 1998, vol. 151}, p. 273-285.
[17] Zemánek, P., Jonáš, A., Šrámek, L., Liška, M. Optical trapping of nanoparticles and microparticles using Gaussian standing wave. *Opt. Lett.* 1999, vol. 24, p. 1448-1450.
[18] Harada, Y., Asakura, T. Radiation forces on a dielectric sphere in the Rayleigh scattering regime. *Opt. Commun.* 1996, vol. 124, p. 529-541.
[19] Tlusty, T., Meller, A., Bar-Ziv, R. Optical gradient forces of strongly localized fields. *Phys. Rev. Lett.* 1998, vol. 81, p. 1738-1741.
[20] Kerker, M. *The Scattering of Light and Other Electromagnetic Radiation*. 1st ed. New York: Academic, 1969. 666p. Physical Chemistry series.
[21] Born, M., Wolf, E. *Principles of optics.* 7th ed. London: Pergamon Press, London, 1999. 952 p. ISBN 0-521-64222-1
[22] Barton, J. P., Alexander, D. R., Schaub, S. A. Internal and near-surface electromagnetic fields for a spherical particle irradiated by a focused laser beam. *J. Appl. Phys.* 1988, vol. 64, p. 1632-1639 .
[23] Barton, J. P., Alexander, D. R., Schaub, S. A. Theoretical determination of net radiation force and torque for a spherical particle illuminated by a focused laser beam. *J. Appl. Phys.* 1989, vol. 66, p. 4594-4602.
[24] Barton, J. P., Alexander, D. R. Fifth-order corrected electromagnetic field components for a fundamental Gaussian beam. *J. Appl. Phys.* 1989, vol. 66, p. 2800-2802.
[25] Rohrbach, A., Stelzer, E. H. K. Optical trapping of dielectric particles in arbitrary fields. *J. Opt. Soc. Am. A* 2001, vol. 18, p. 839-853.
[26] Pralle, A., Prummer, M., Florin, E.-L., Stelzer, E. H. K., Horber, J. K. H. Three-dimensional high-resolution particle tracking for optical tweezers by forward scattered light. *Micr. Res. Techn.* 1999, vol. 44, p. 378-386.
[27] Friese, M. E. J., Rubinsztein-Dunlop, H., Heckenberg, N. R., Dearden, E. W. Determination of the force constant of a single-beam gradient trap by measurement of backscattered light. *Appl. Opt.* 1996, vol. 35, p. 7112-7116.
[28] Mandel, L., Wolf, E. *Optical coherence and quantum optics*, 1st ed. Cambridge: Cambridge University Press, 1995. 1166 p. ISBN 0-521-41711-2
[29] Florin, E.-L., Pralle, A., Stelzer, E. H. K., Horber, J. K. H. Photonic force microscope calibration by thermal noise analysis. *Appl. Phys. A* 1998, vol. 66, p. 75-78.
[30] Pralle, A., Florin, E.-L., Stelzer, E. H. K, Horber, J. K. H. Local viscosity probed by photonic force microscopy. *Appl. Phys. A* 1998, vol. 66, p. 71-73.
[31] Wright, W. H., Sonek, G. J., Berns, M. W. Parametric study of the forces on microspheres held by optical tweezers. *Appl. Opt.* 1994, vol. 33, p. 1735-1748.
[32] Press, W., Teukolsky, S., Vetterling, W., Flannery, B. *Numerical recipes in C*, 2nd ed. Cambridge: Cambridge University Press, 1992. 994 p. ISBN 0-521-43108-5

[33] Florin, E.-L., Horber, J. K. H., Stelzer, E. H. K. High-resolution axial and lateral position sensing using two-photon excitation of fluorophores by a continuous wave Nd:YAG laser. *Appl. Phys. Lett.* 1996, vol. 69, p. 446-448.

7 CURRICULUM VITAE

Mgr. Alexandr Jonáš

Date and place of birth: 15th December 1972, Valtice

1996 - graduation from Masaryk university in Brno, Faculty of Sciences, academic degree Mgr. (MSc.) in biophysics - diploma thesis: „Model interakce elektromagnetického záření s malými objekty."
1996 - internal Ph.D. student at the Institute of Physical Engineering, Faculty of Mechanical engineering, Brno University of Technology; part-time employment at the Department of Coherence Optics, Institute of Scientific Instruments, Academy of Sciences of the Czech Republic
1999 - Ph.D. course finished with the state rigorous exam, defence of the Ph.D. thesis outline – title: „Use of standing electromagnetic wave for manipulation of micron and submicron-sized objects"; full-time employment at the Institute of Scientific Instruments, ASCR

Professional activities

Laser manipulation of microobjects – theory, experiment and applications:
- calculation of the forces acting on objects confined in light beams
- experimental realisation of the optical manipulation system
- measurement of the optical traps' parameters
- application of micromanipulation techniques for the study of the properties of cells, cell nuclei or single macromolecules

Visits in foreign laboratories:

1997 - IMB Jena a PTB Braunschweig, Germany (7 days) – introduction to the research projects solved at the top European laboratories (single molecule studies, development of laser frequency standards, local probe microscopes)
2000 - Tohoku University (Sendai, Japan), National Institute of Genetics (Mishima, Japan), Osaka University (Osaka, Japan) – invited lecture *"Comparison of microobjects optical trapping by single beam and standing wave"*
2000 - EMBL Heidelberg, Germany (3 months) – EMBO fellowship, common project with Light Microscopy Group (analysis of the standing wave trap)